THE STRUCTURE OF MOTION IN A 4-COMPONENT GALAXY MASS MODEL

N.D. CARANICOLAS
Department of Physics, Section of Astrophysics, Astronomy and Mechanics, University of Thessaloniki, 540 06 Thessaloniki, Greece

(Received 3 October, 1996; accepted 18 December, 1996)

Abstract. We use a composite galaxy model consisting of a disk-halo, bulge, nucleus and dark-halo components in order to investigate the motion of stars in the $r - z$ plane. It is observed that high angular momentum stars move in regular orbits. The majority of orbits are box orbits. There are also banana-like orbits. For a given value of energy, only a fraction of the low angular momentum stars – those going near the nucleus – show chaotic motion while the rest move in regular orbits. Again one observes the above two kinds of orbits. In addition to the above one can also see orbits with the characteristics of the 2/3 and 3/4 resonance. It is also shown that, in the absence of the bulge component, the area of chaotic motion in the surface of section increases significantly. This suggests that a larger number of low angular momentum stars are in chaotic orbits in galaxies with massive nuclei and no bulge components.

1. Introduction

In an earlier paper (see Caranicolas and Innanen, 1991) we have studied the behaviour of the low angular momentum stars in a galaxy with a disk-halo and a massive nucleus components. We found that there is a well-defined transition from regular motion to chaos, for a given mass of the disk-halo component.

In the present paper we shall use a composite, axially symmetric galaxy model, in order to study the motion of stars in the meridional plane of the galaxy. The galaxy potential consists of four components. The first component is the disk-halo component represented by the potential

$$\Phi_{dh}(r,z) = -\frac{M_{dh}}{R}, \tag{1}$$

with

$$R^2 = \left[\alpha + \sum_{i=1}^{3} \beta_i \sqrt{z^2 + h_i^2}\right]^2 + b^2 + r^2. \tag{2}$$

Here r, z are cylindrical coordinates, M_{dh} is the mass, α, h are the scale length and the scale height of the disk respectively while b is the core radius of the halo component. β_1, β_2, β_3 represent the fractional portions of old disk, dark matter and young disk respectively. The other three components are represented by the spherically symmetric potentials

Astrophysics and Space Science **246:** 15–28, 1997.

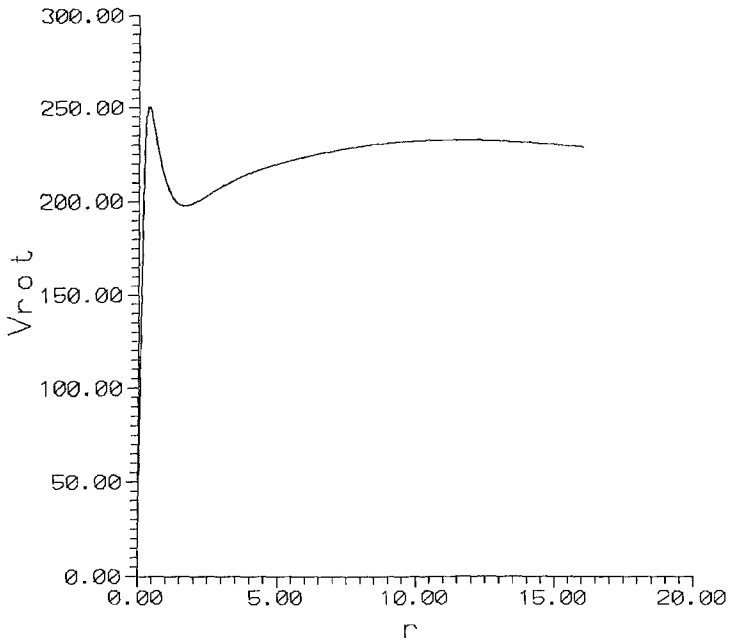

Figure 1. The rotation curve for the model galaxy.

$$\Phi_n = -\frac{M_n}{[r^2+z^2+c_n^2]^{1/2}},\ \Phi_b = -\frac{M_b}{[r^2+z^2+c_b^2]^{1/2}},\ \Phi_h = -\frac{M_h}{[r^2+z^2+c_h^2]^{1/2}}, \tag{3}$$

where M_n, M_b, M_h are the mass of the nucleus, bulge and dark halo, respectively, while c_n, c_b, c_h are the corresponding scale lengths. As in Caranicolas and Innanen (1991) we shall use a system of galactic units where the unit of length is 1 kpc, the unit of mass is $2.325 \times 10^7\ M_\odot$ and the unit of time is 0.97748×10^8 yr. The velocity unit is 10 km/s while $G = 1$. Using these units we take $M_{dh} = 9350$, $M_n = 400$, $M_b = 2000$, $M_h = 11500$, $\alpha = 3.1$ kpc, $b = 10$ kpc, $(\beta_1, \beta_2, \beta_3) = (0.4, 0.5, 0.1)$, $(h_1, h_2, h_3) = (0.325, 0.090, 0.125)$ kpc, $c_n = 0.25$ kpc, $c_b = 3$ kpc, $c_h = 40$ kpc. The rotation curve $V_{rot} = V_{rot}(r)$ of our galactic model is shown in Figure 1. One can see that the rotational velocity at $r = 8.5$, $z = 0$ – which is considered as the position of the Sun in our Galaxy – is 230 km/s. It is found that the corresponding total mass density at the same point is $0.182\ M_\odot/\text{pc}^3$ while the total mass of the model is $5.4 \times 10^{11}\ M_\odot$. Therefore one can say that the above galaxy model describes a galaxy similar to our Galaxy (see also Carlberg and Innanen, 1987 and references therein).

The purpose of this work is to study the properties of motion in the above galaxy model. In particular we shall study: (i) The kind of motion (regular or chaotic) for different values of the angular momentum. (ii) The different kinds of orbits (box orbits, loop orbits etc.) that are met in the galaxy. (iii) How this picture of motion is

affected by the presence or absence of the various components, that is the particular structure of the galaxy.

The present article is organized as follows: After presenting the galaxy model (Section 1) we use numerical integration in order to find the behaviour of the orbits (Section 2). In Section 3 we study the behaviour of the orbits using a galactic model without the halo or bulge components. Finally a discussion and the conclusions of this work are presented in Section 4.

2. Orbital Characteristics when all Galactic Components are Present

The Hamiltonian describing the motion in the $r-z$ plane is

$$H=\frac{1}{2}[p_r^2+p_z^2]+\Phi_{eff}(r,z)=E, \tag{4}$$

where p_r, p_z are the momenta per unit mass conjugate to r, z, E is the numerical value of H while

$$\Phi_{eff}=\frac{L_z^2}{2r^2}+\Phi_{tot}, \tag{5}$$

$\Phi_{tot}=\Phi_{dh}+\Phi_n+\Phi_b+\Phi_h$, and L_z is the component of the angular momentum about the z-axis. The equations of motion read

$$\ddot{r}=-\frac{\partial\Phi_{eff}}{\partial r},\ \ddot{z}=-\frac{\partial\Phi_{eff}}{\partial z}. \tag{6}$$

In the following we shall make an extensive study of the motion in our model galaxy using the traditional method of the Poincare surface of section, i.e. the $r-p_r$ $(z=0, p_z>0)$ surface of section. Figure 2 shows the surface of section of the model when $E=-976$, $L_z=180$. The value of the energy E was found as follows. First we compute the value Φ_{eff} at the point $(r,z)=(8.5,0)$ using the value of angular momentum $L_{oz}=L_{zci}=195.5$ which is the value of the circular angular momentum at $r=8.5$. Let this value be E_{eff}. Then we choose as $E=E_{eff}$ dropping the decimal points. The value of $L_z=180$ is about 8% smaller than L_{zci}. This smaller values was chosen in order to obtain the desirable area of motion in the $r-z$ plane.

As we can see, in Figure 2, the surface of section is covered by invariant curves, therefore the motion is regular. Two kinds of orbits are present, the banana-like orbits and the box-orbits. The first kind of orbits produce the islands on the surface of section while the second kind of orbits produce the rest of the invariant cuves. Figure 3 shows a banana-like orbit when $E=-976$, $L_z=180$. A box orbit, for the same values of E, L_z is shown in Figure 4. The outermost thick curve in all orbit Figures is the curve of zero velocity. This can be found solving numerically the equation

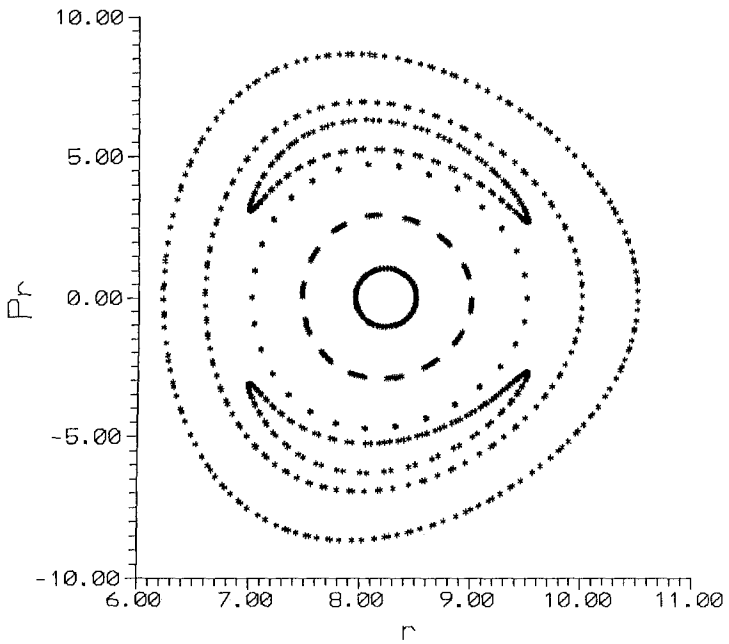

Figure 2. The $r - p_r$ surface of section when $E = -976$, $L_z = 180$.

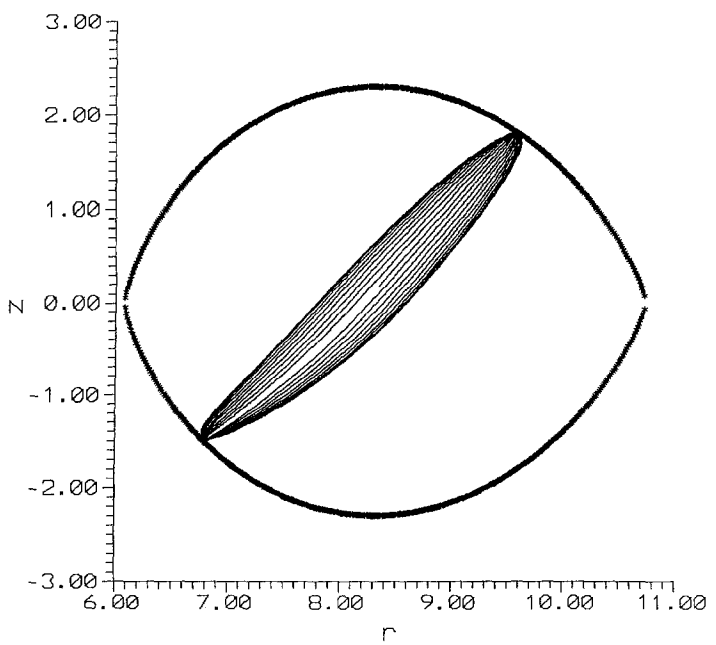

Figure 3. A banana-like orbit. The outermost curve is the curve of zero velocity. The values of E, L_z are as in Figure 2.

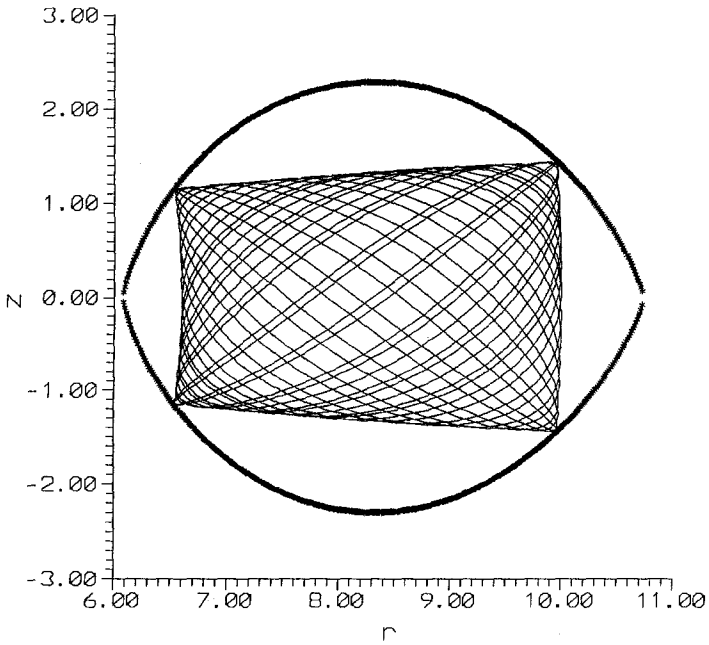

Figure 4. A box orbit. The outermost curve is the curve of zero velocity. The values of E, L_z are as in Figure 2.

$$\Phi_{eff}(r,z) - E = \frac{L_z^2}{2r^2} + \Phi_{tot}(r,z) - E = 0. \tag{7}$$

Figure 5 shows the surface of section when $L_z = 50$, $E = -1217$. The value of energy was found as above using a value of angular momentum $L_{zo} = 0.3L_{zci} = 58.65$. Here again the motion is regular except for the outer part of the surface of section where chaotic motion is observed. It is evident that the orbits forming the chaotic layer are those going near the nucleus as one can see in Figure 5. The minimum and maximum value of r can be found by solving numerically the equation

$$\Phi_{eff}(r,0) - E = \frac{L_z^2}{2r^2} + \Phi_{tot}(r,0) - E = 0. \tag{8}$$

For the case of Figure 5 we find $r_{\max} = 8.6192$, $r_{\min} = 1.1737$ while for Figure 2 we have $r_{\max} = 10.7211$, $r_{\min} = 6.0819$.

Going to even smaller values of the angular momentum we get the surface of section shown in Figure 6. Here we have $E = -1238$, $L_z = 15$. The value of energy is found as above with $L_{zo} = 0.1L_{zci} = 19.5$. It is evident that here we observe a larger chaotic layer. Again the chaotic orbits are the orbits going very close to the nucleus. In this case, from Equation (8) we find $r_{\max} = 8.5266$, $r_{\min} = 0.2557$. The majority of orbits are regular orbits. The regular orbits are three kinds. Box orbits, banana-like orbits and orbits characteristic of the 2/3 resonance. These orbits give

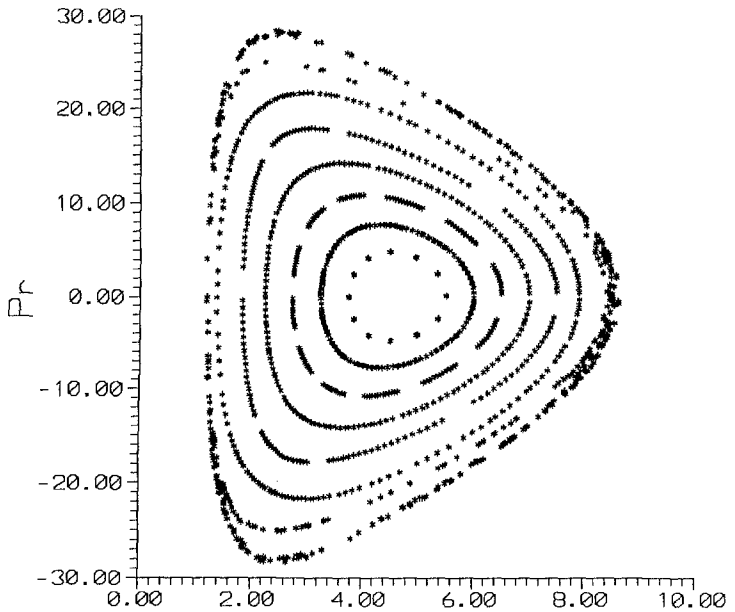

Figure 5. The $r - p_r$ surface of section when $E = -1217$, $L_z = 50$.

the two sets of small islands in Figure 6 while the elongated islands are produced by the banana-like orbits. A quasi-periodic orbit characteristic of the 2/3 resonance is shown in Figure 7. The values of E, L_z are as in Figure 6.

Figure 8 shows a chaotic orbits while Figure 9 shows the time evolution of the z-component of the same orbit for 100 time units. The values of E, L_z are as in Figure 6. Looking at those Figures one observes two interesting results: (i) the star goes to higher z only when the galactocentric distance r is more than about 2 kpc and (ii) after its deflection to higher z, there are also time intervals where the star returns and stays near the disk. We shall come to that point again in the next section.

3. Orbital Characteristics Without the Halo or Bulge Components

In what follows we shall see the phase-space portrait of orbits when one or more components of our composite model are not present. Let us start when both halo and disk halo components are absent. The corresponding surface of section for our galaxy model with the nucleus, bulge and disk is given in Figure 10. The value of energy, which was found as in the case of Figure 6, is $E = -1290$ while $L_z = 15$. Here we find $r_{\max} = 8.5248$, $r_{\min} = 0.1788$. One observes that the picture is similar to that of Figure 6 with some minor changes. (i) There is a small increase in the chaotic area. (ii) So are the islands corresponding to banana-like orbits. (iii)

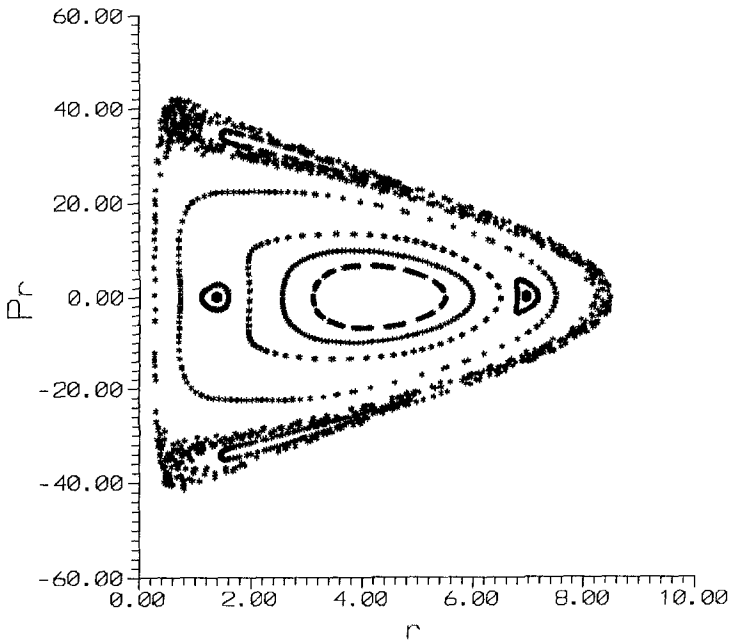

Figure 6. The $r - p_r$ surface of section when $E = -1238$, $L_z = 15$.

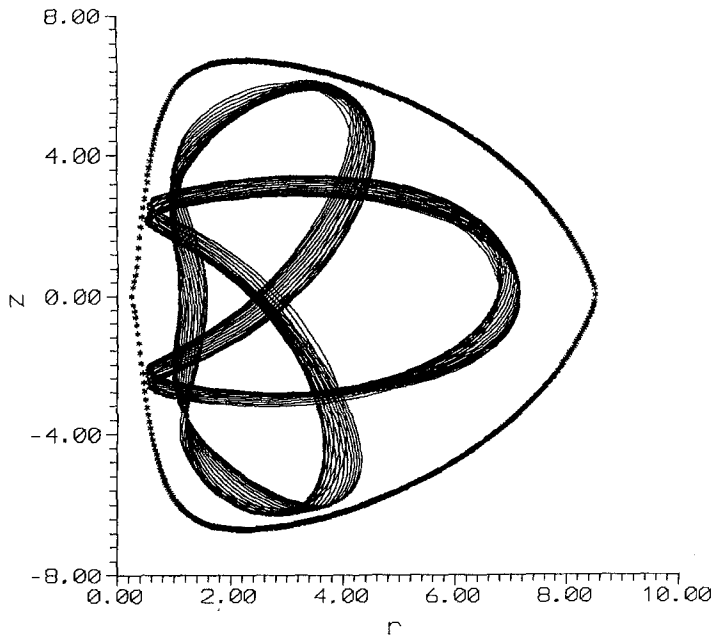

Figure 7. A quasi-periodic orbit. The system is near 2/3 resonance. The values of E, L_z are as in Figure 6.

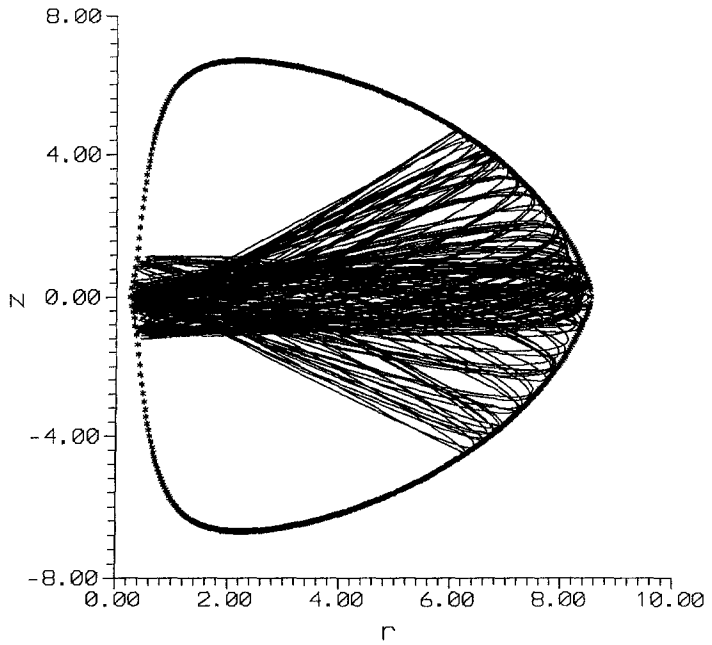

Figure 8. A chaotic orbit. The values of E, L_z are as in Figure 6. The outermost curve is the curve of zero velocity.

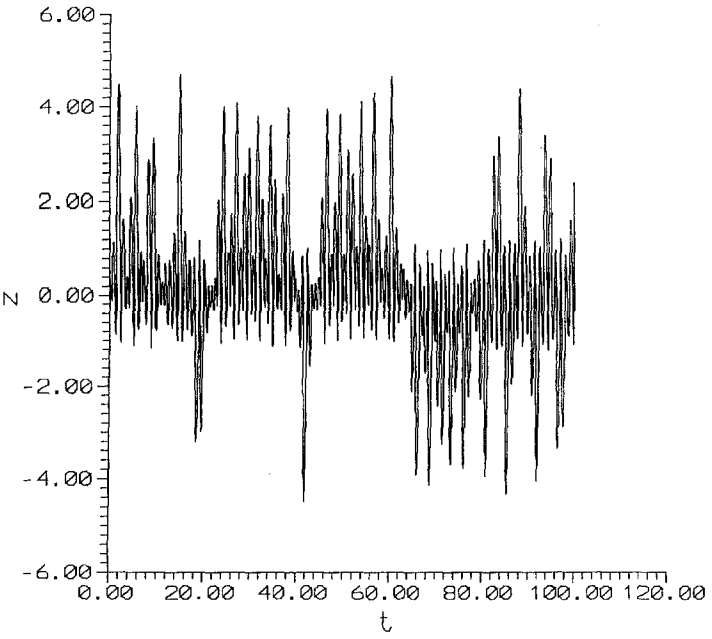

Figure 9. Evolution of the star's z-height with the time for the orbit of Figure 8.

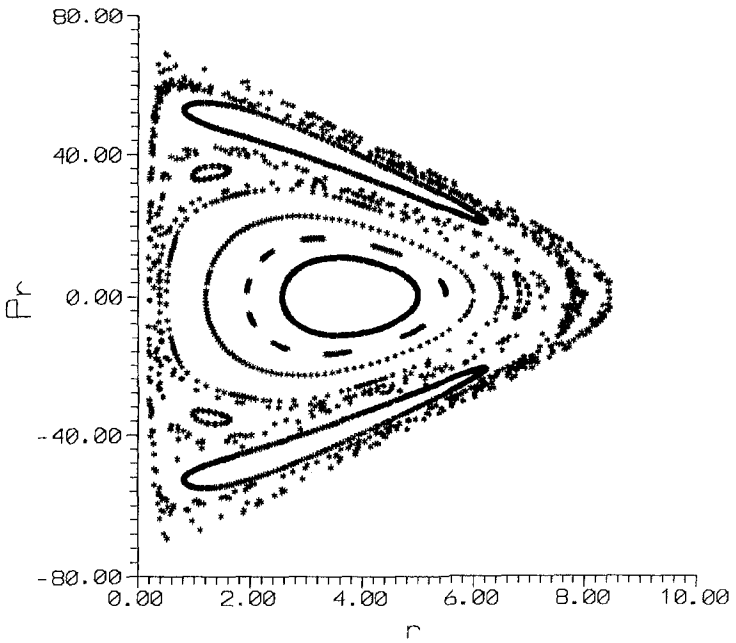

Figure 10. The $r - p_r$ surface of section when $E = -1290$, $L_z = 15$. The system has no halo components.

Instead of a set of 2 islands we have a set of 3 small islands corresponding to a quasi periodic orbit characteristic of the 4/3 resonance. Figure 11 shows the time evolution of the z-component of a chaotic orbit for 100 time units. As we can see the maximum z is about 1.5 kpc. This result suggests that, in the absence of the halo components, stars approaching the nucleus move in chaotic orbits practically staying near the galactic plane.

The phase-space portrait of the system when all components, except the bulge component, are present is shown in Figure 12. The value of energy, computed as in the case of Figure 6, is $E = -1016$ while $L_z = 15$. Here we find $r_{\max} = 8.5456$, $r_{\min} = 0.3112$. It is clear that less than 50% of the surface of section is covered by invariant curves while the rest form a large chaotic area. We see again the same three kinds of orbits as described in Figure 10. Figure 13 shows a chaotic orbit when $E = -1016$, $L_z = 15$. The integration time was 100 time units. The difference with the orbit of Figure 8 is obvious. We observe that the orbit is deflected to the halo although it is started at $r = 8.5$, $z = 0$, with a vertical velocity less than 20 km/s. Another characteristic of this orbit is that it covers almost all the permissible area inside the zero velocity curve. Figure 14 shows the time evolution of the z component for 100 time units. It is easy to see that the star spends long time intervals in high values of z especially for $t > 60$ time units.

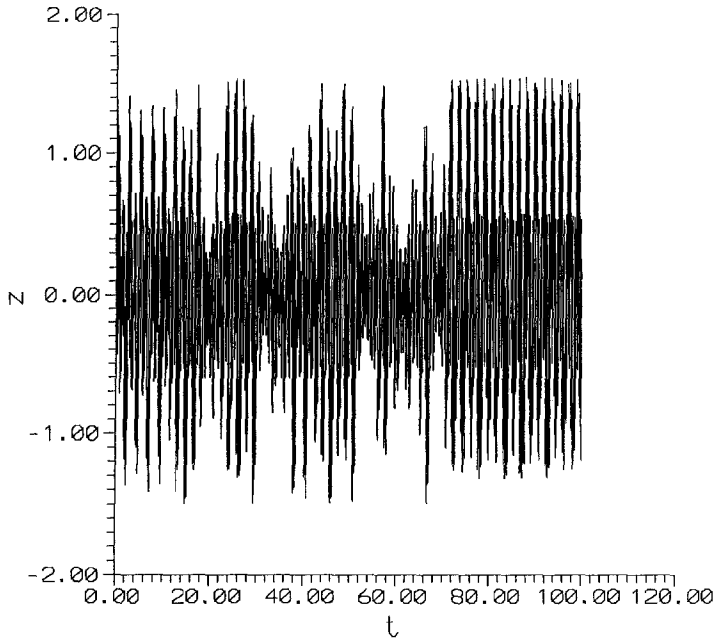

Figure 11. Evolution of the star's z-height with the time for an orbit in the case when the halo components are not present. The values of E, L_z are as in Figure 10.

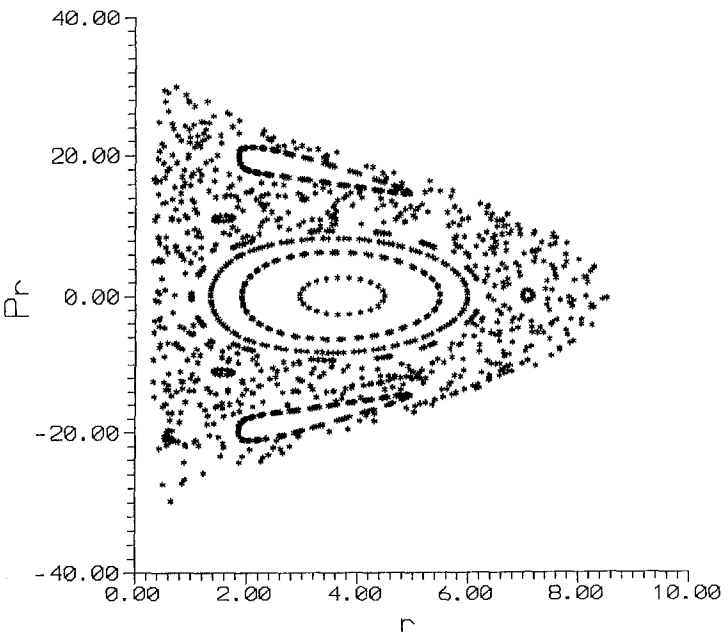

Figure 12. The $r - p_r$ surface of section when $E = -1016$, $L_z = 15$. The system has no bulge component.

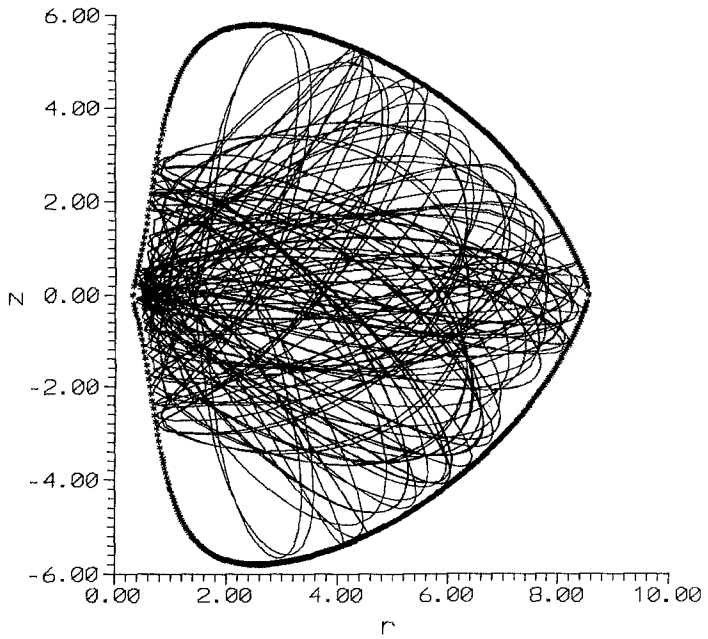

Figure 13. A chaotic orbit when the bulge component is not present. The values of E, L_z are as in Figure 12. The outermost curve is the curve of zero velocity.

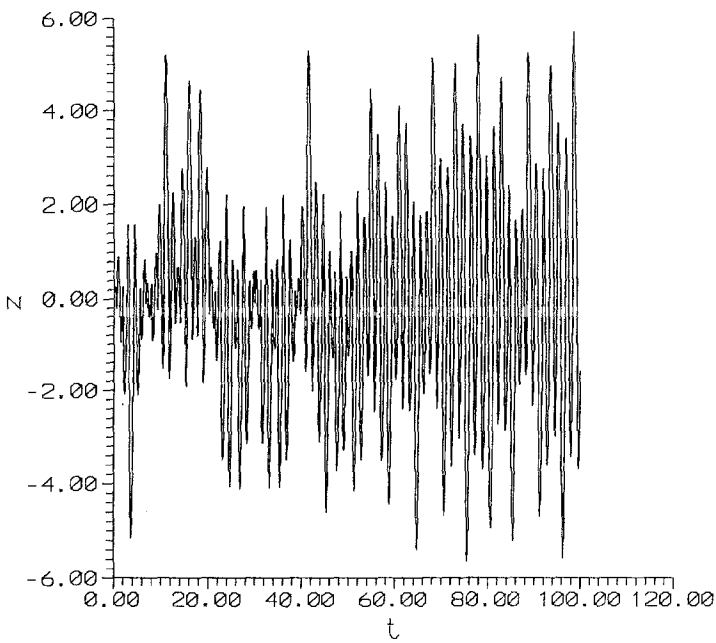

Figure 14. Evolution of the star's z-height with the time for the orbit of Figure 13.

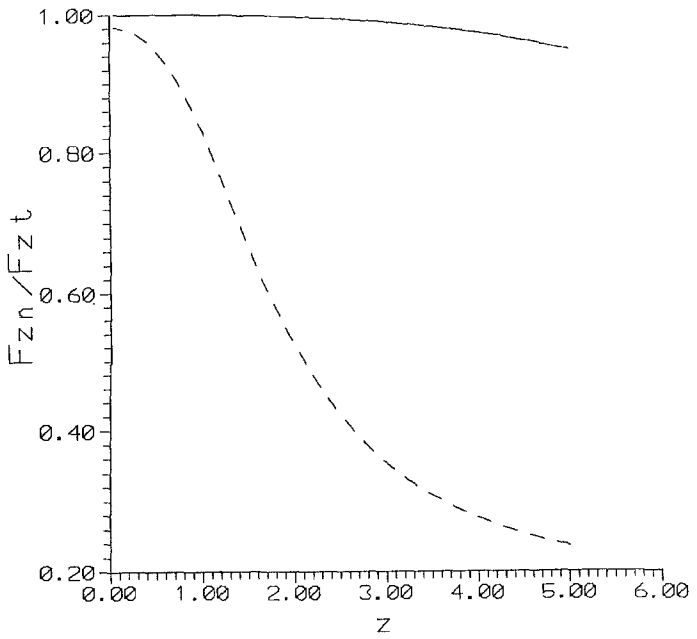

Figure 15. The ratio of the nuclear F_{zn} to the total F_{zt} z-force with (dashed line) and without (solid line) the bulge component.

If one compares the case of Figure 12 with those of Figures 6 and 10 it is reasonable to ask: Why in the absence of the bulge component is there a large increase of the chaotic region? The answer comes from Figure 15. In this Figure we give the ratio of the nuclear z-force to the total z-force F_{zn}/F_{zt} as a function of z, for a fixed value of r near the nucleus (here $r = 0.4$). The solid line is for the model without the bulge while the dashed line is with the bulge component. It is evident that in the case where the bulge component is not present, the nuclear z-force, which is responsible for the scattering of the star and the chaotic motion (see Caranicolas and Innanen, 1991), is almost equal to the total force (even at $z = 5$ is about 95% of F_{zt}) and therefore produces a much larger chaotic region.

4. Discussion

In order to study the properties of motion in galaxies astronomers use a variety of models. Two of the basic kinds of models are mass models of the above kind and the perturbed harmonic oscillators model. As it is well known, the first category of models sescribes global motion while the second category describes local motion. Mass models were used by several investigators (see Clutton Brock *et al.*, 1977; Carlberg and Innanen, 1987; Caranicolas and Innanen, 1991) while the perturbed harmonic oscillators have been extensively used during the last three decades (see

e.g. Caranicolas, 1990, 1993, 1994; Caranicolas and Innanen, 1992; Caranicolas and Barbanis, 1982; Innanen, 1985; Deprit, 1991).

The numerical calculations suggest that for our composite galaxy model the motion is regular when $L_z > 50$. The first signs of chaotic motion appear at $L_z = 50$. For this critical value of the angular momentum the consequents of the orbits going near the nucleus produce a thin stochastic layer instead of forming invariant curves. It is common in dynamical astronomy to call those orbits stochastic orbits or chaotic orbits. The author would like to note here that numerical calculations not given here show that for the same value of energy ($E = -1217$) and $L_z = 55$ the motion is regular. Therefore the first signs of chaos appear when $55 < L_z \leq 50$. We did not feel it was necessary to find the value of L_z with more accuracy.

As a general conclusion we can say that there are two main kinds of orbits in our model galaxy. (i) Box orbits which represent the majority of orbits and (ii) banana-like orbits. The above two kinds of orbits exist both for high and low values of L_z as well as when several galactic components are absent. In addition to the above orbits resonant orbits appear for low values of the angular momentum. The observed orbits have the characteristics of the 2/3 or the 4/3 resonances.

In order to see the properties of the orbits of the low angular momentum stars we have chosen a value of $L_z = 15$, much smaller than the critical value, in order to have a large enough chaotic region. It is reasonable for this chaotic region to change when the structure of the model galaxy changes. The most interesting change is the extension of the chaotic region when the system has no bulge component. As was mentioned before, in the absence of bulge, the star, upon encountering the nuclear region, experiences a nuclear z-force which is nearly equal to the total z-force even at large z. Therefore our numerical work suggests that the presence of the bulge component reduces the degree of chaos in our model galaxy.

At this point we must notice that there are cases where the bulge itself produces chaos. As it is indicated in Caranicolas and Innanen (1991) the bulge produces chaos only in the cases where $c_b < 1.3$ kpc. This result is independent of the mass of the bulge. In other words chaos is produced by the bulge only with a relative high mass concentration. Here we have $c_b = 3$ kpc, and therefore we do not expect the bulge to produce chaos. On the contrary we observe that the bulge reduces the width of the chaotic layer (compare Figures 6 and 12).

On the other hand, we observe that the absence of the halo components produces a small increase in the degree of chaos (compare Figures 6 and 10). Numerical results not given here suggest that there is a small increase in the ratio F_{zn}/F_{zt} caused by the absence of the halo components. This small increase together with the fact that the star goes closer to the nucleus, when the bulge component are not present, is responsible for the small increase of the chaotic area. An interesting result noticed here is that in the absence of the halo components, the star prefers to orbit near the plane of the galaxy while in the presence of the halo components the star goes to much higher values of z (compare Figures 9 and 11).

The numerical calculations were made by means of a Bulirsh-Stoer method in double precision. The time scale for the calculation of each orbit in the $r - z$ or $z - t$ plane was 50–100 time units while the time scale for each orbit in the surface of section was 500–1000 time units. The values of the energy E and angular momentum were taken such as to cover a representative part of the $r - z$ plane in our galaxy model. Note that in all cases the value of the angular momentum, used for the computation of orbits, was smaller to that (L_{zo}) used to compute the value of energy E. This was done in order to increase the distance $r_{\max} - r_{\min}$.

References

Caranicolas, N.D.: 1990, *Cel. Mech.* **47**, 87.
Caranicolas, N.D.: 1993, *Astron. Astrophys.* **267**, 388.
Caranicolas, N.D.: 1994, *Astron. Astrophys.* **291**, 754.
Caranicolas, N.D. and Barbanis, B.: 1982, *Astron. Astrophys.* **114**, 360.
Caranicolas, N.D. and Innanen, K.A.: 1991, *Astron. J.* **102**, 1343.
Caranicolas, N.D. and Innanen, K.A.: 1992, *Astron. J.* **103**, 1308.
Carlberg, R.G. and Innanen, K.A.: 1987, *Astron. J.* **94**, 667.
Clutton-Brock, M., Innanen, K.A. and Papp, K.A.: 1977, *Astrophys. Space Sci.* **47**, 299.
Deprit, A.: 1991, *Celest. Mech. Dyn. Astron.* **51**, 201.
Innanen, K.A.: 1985, *Astron. J.* **90**, 2377.